Crystal-field and Kondo-scale investigations of CeMIn$_5$ (M=Co, Ir, and Rh): A combined x-ray absorption and inelastic neutron scattering study

T. Willers,[1] Z. Hu,[1,2] N. Hollmann,[1] P. O. Körner,[1] J. Gegner,[1] T. Burnus,[1,*] H. Fujiwara,[1] A. Tanaka,[3] D. Schmitz,[4] H. H. Hsieh,[5] H.-J. Lin,[6] C. T. Chen,[6] E. D. Bauer,[7] J. L. Sarrao,[7] E. Goremychkin,[8] M. Koza,[9] L. H. Tjeng,[1,2] and A. Severing[1]

[1]*Institute of Physics II, University of Cologne, Zülpicher Straße 77, D-50937 Cologne, Germany*
[2]*Max Planck Institute CPfS, Nöthnizer Straße 40, 01187 Dresden, Germany*
[3]*Department of Quantum Matter, ADSM Hiroshima University, Higashi-Hiroshima 739-8530, Japan*
[4]*Helmholtz-Zentrum Berlin, BESSY II, Albert-Einstein-Straße 15, D-12489 Berlin, Germany*
[5]*Chung Cheng Institute of Technology, National Defense University, Taoyuan 335, Taiwan*
[6]*National Synchrotron Radiation Research Center (NSRRC), 101 Hsin-Ann Road, Hsinchu 30077, Taiwan*
[7]*Los Alamos National Laboratory, Los Alamos, New Mexico 87545, USA*
[8]*ISIS, Rutherford Appleton Laboratory, Chilton, Didcot, Oxon OX11 0QX, United Kingdom*
[9]*Institut Laue Langevin, 6 rue Horowitz, 38042 Grenoble, France*

(Received 25 February 2010; revised manuscript received 28 April 2010; published 19 May 2010)

Linear-polarized soft-x-ray absorption (XAS) and inelastic neutron scattering (INS) experiments have been performed on CeMIn$_5$ with M=Rh, Ir, and Co to determine the crystal-field scheme and characteristic Kondo temperatures T^* for the hybridization between 4f and conduction electrons. The ground-state wave functions are determined from the polarization-dependent soft-XAS data at the cerium $M_{4,5}$ edge and the crystal-field splittings from INS. The characteristic temperature T^* has been determined from the line widths of the neutron scattering data. We find that the quasielastic linewidths of the superconducting compounds CeCoIn$_5$ and CeIrIn$_5$ are comparable with the low-energy crystal-field splitting.

DOI: 10.1103/PhysRevB.81.195114 PACS number(s): 71.27.+a, 75.10.Dg, 78.70.Dm, 78.70.Nx

I. INTRODUCTION

The ternary rare-earth family CeMIn$_5$ (M=Co, Ir, and Rh) are heavy-fermion, unconventional superconductors:[1,2] CeCoIn$_5$ and CeIrIn$_5$ become superconducting at ambient pressure at T_c=2.3 (Ref. 1) and T_c=0.4 K (Ref. 3) whereas the incommensurate heavy fermion antiferromagnet CeRhIn$_5$ (T_N=3.8) exhibits superconductivity under pressure (P_c =1.6 GPa, T_c=2.1 K).[4] All members of this family crystallize in the tetragonal HoCoGa$_5$ structure (space group $P4/mmm$), which is derived from cubic CeIn$_3$ intercalated with MIn$_2$ layers along the tetragonal c axis. The cubic compound CeIn$_3$ orders antiferromagnetically at T_N=10 K and has a hybridization temperature T^* of about 10 K.[5] This temperature, which gives the energy scale of the hybridization between the local 4f moments and surrounding conduction electrons, is highly pressure-dependent in CeMIn$_5$ compounds. It has been argued that a sufficiently strong hybridization or Kondo interaction with respect to the RKKY (Ruderman-Kittel-Kasuya-Yosida) exchange interaction suppresses antiferromagnetic order to the benefit of superconductivity.[6–8] General scaling behaviors of the characteristic energy scales in Kondo lattice materials are a matter of intense debate[9–12] and T^* has traditionally been interpreted as the temperature below which the coherence of the Kondo lattice sets in. More recently T^* has been suggested to be the temperature scale denoting the development of a dense "Kondo liquid" within a "two-fluid" model also comprised of a "Kondo gas" phase of uncorrelated magnetic moments at high temperatures. This characteristic temperature scale is determined with many techniques such as thermodynamic, transport, knight-shift measurements, and of course, quasielastic neutron scattering.[13–17] Another interesting scaling has been shown by Bauer *et al.*:[18] the superconducting transition temperatures T_c of the CeMIn$_5$ and also of the PuMGa$_5$ family vary linearly with the c/a ratio of the tetragonal lattice constants, pointing toward the importance of the anisotropic electronic structure for the superconducting state. This brings into focus the importance of the spatial distribution of the crystal-field (CF) split Hund's rule ground state, which is highly anisotropic for materials containing rare earth.

The Hund's rule ground state of Ce^{3+} with $J=5/2$ splits under the influence of a tetragonal crystal-field (point group D_{4h}) into three Kramer's doublets, which can be represented in the basis of $|J_z\rangle$. The eigenfunctions of the three Kramer's doublets can be written as

$$|2\rangle = \Gamma_6 = |\pm 1/2\rangle,$$

$$|1\rangle = \Gamma_7^1 = \beta|\pm 5/2\rangle - \alpha|\mp 3/2\rangle,$$

$$|0\rangle = \Gamma_7^2 = \alpha|\pm 5/2\rangle + \beta|\mp 3/2\rangle \quad (1)$$

with $\alpha^2+\beta^2=1$. The anisotropy of certain wave functions may give rise to 4f conduction electron hybridizations which are more advantageous than others for forming a superconducting ground state.[19] The importance of momentum-dependent (**q**-dependent) hybridization in these and some semiconducting Kondo materials has been investigated by several groups.[20–26]

Various groups attempted to determine the crystal-field scheme of these compounds, but there are significant discrepancies depending on the applied methods, which include

TABLE I. Experimental details about the XAS measurements.

Sample	Synchrotron facility	Sequence of temperatures (K)
$CeCoIn_5$ 1	NSRRC	78,12, 295
$CeCoIn_5$ 2	NSRRC	10
$CeCoIn_5$ 3	BESSY	18, 50, 80, 130, 17, 180, 280, 17, recleave, 19, 50, 80, 280
$CeIrIn_5$ 1	NSRRC	18, 50, 80, 150, 300, recleave, 300
$CeRhIn_5$ 2	NSRRC	20, 80, 295
$CeRhIn_5$ 2	BESSY	18, 50, 80, 150, 300

bulk measurements based on transport, thermodynamic, and NMR experiments.[19,27–30] Christianson *et al.*[31,32] performed extensive inelastic neutron scattering (INS) studies but phonon contributions in the energy range of the magnetic scattering broadened crystal-field excitations due to hybridization effects and the enormous absorption of the sample's constituents make the determination of reliable magnetic intensities rather challenging. Since the latter give the wave functions via the transition-matrix elements the resulting wave functions should be taken with care (see appendix) while the transition energies are fairly sound (see Sec. III B).

We have shown for the case of the heavy fermion materials $CePd_2Si_2$ and $CePt_3Si$ that polarization dependent soft x-ray absorption (XAS) at the Ce $M_{4,5}$ edges can be complementary to neutron scattering in determining the ground-state wave function.[33,34] XAS is highly sensitive to the initial state and via its polarization dependence (*linear dichroism* LD) direct information about the $|J_z\rangle$ admixtures of the ground-state wave function can be obtained. Sensitivity to higher-lying crystal-field states is achieved by thermally populating those states.[33,34]

We present a combined inelastic neutron scattering and soft x-ray absorption study on the $CeMIn_5$ M=Co, Ir, and Rh compounds. Combining both techniques has the advantage of determining transition energies and mixing parameters independently, each with the most suitable technique. The line positions in the magnetic contributions of the INS data yield the crystal-field transition energies within meV resolution, whereas the LD in XAS, when performed at temperatures where only the ground state is populated, yields the ground-state wave function, i.e., in case of a mixed ground state the mixing factor α^2 [see Eq. (1)] within $\Delta\alpha^2 = \pm 0.0025$. In the limit of small crystal-field splittings the dichroic signal of the ground state is independent of crystal-field energies. Once the ground state has been determined, the order of states can be determined from the temperature dependence of the LD since at finite temperatures it reflects the superposition of polarizations from each populated state, i.e., here the crystal-field energies, as determined from the neutron scattering experiment, enter via the thermal population. In addition, high-resolution INS data are presented to determine the characteristic temperature T^* for the $4f$ conduction electron hybridization via the quasielastic linewidth. The latter has been applied successfully by several authors.[13,15–17]

II. EXPERIMENTAL AND DATA CORRECTION

The high-quality single crystals of $CeMIn_5$ for the x-ray experiments were grown with the flux-growth method.[6] The powder samples for the present INS experiments were the same samples as used by Christianson *et al.*[31,32]

A. XAS

The XAS spectra were recorded during various beam times at the two different synchrotron light sources BESSY II and NSRRC. We recorded all spectra with the total electron yield (TEY) method and under UHV, i.e., in a chamber with a pressure in the 10^{-10} mbar range. Clean sample surfaces were obtained by cleaving the samples *in situ*. At BESSY II we used the UE46 PGM-1 undulator beam line. The TEY signal was normalized to the incoming photon flux I_0 as measured at the refocusing mirror. The energy resolution at the cerium $M_{4,5}$ edges ($h\nu \approx 875-910$ eV) was set to 0.15 eV. The undulator combined with a normal incident measurement geometry allow for a change in polarization without changing the probed spot on the sample surface. The two polarizations were $E \perp c$ and $E \| c$, c being the long tetragonal axis. At the NSRRC we performed the experiment at the Dragon dipole beam line. The energy resolution at the cerium $M_{4,5}$ edges was set to 0.4 eV. The crystals were mounted with the c axis perpendicular to the Poynting vector of the light. By rotating the sample around this Poynting vector, the polarization of the electric field can be varied continuously from $E \perp c$ to $E \| c$. For all measurements the sample was rotated 4 times by 90° so that for each orientation $E \perp c$ and $E \| c$ two equivalent positions were measured. Thus for both experimental end stations a reliable comparison of the spectral line shapes is guaranteed. We measured several crystals and/or recleaved in order to assure the reproducibility of the spectra (see Table I).

To calculate the XAS spectra we performed ionic full multiplet calculations using the XTLS 8.3 program.[35] All atomic parameters are given by Hartree-Fock values with a reduction of about 40% for the $4f$-$4f$ Coulomb interactions and about 20% for the $3d$-$4f$ interactions to reproduce best the experimental isotropic spectra, $I_{\text{isotropic}} = 2I_{\perp} + I_{\|}$. These values compare well with our findings for other heavy-fermion compounds[33,34] and account for the configuration interaction effects not included in the Hartree-Fock scheme.

Once the atomic parameters are fine tuned to the isotropic spectra, the polarized XAS data can be described by the incoherent sums of the respective polarization-dependent spectra of the pure $|J_z\rangle$ states[33] as long as the crystal-field splitting E_{CF} is small with respect to the spin orbit splitting E_{SO}. The latter requirement, which is fulfilled here ($E_{SO} \approx 280$ meV and $E_{CF} \leq 30$ meV), assures that interference terms resulting from intermixing of the $J=5/2$ and $J=7/2$ multiplet can be neglected.

B. Inelastic neutron scattering

We have measured the neutron-scattering function $S(Q,\omega)$ of $CeRhIn_5$, $CeIrIn_5$, and $CeCoIn_5$ with the inelastic time-of-flight high energy transfer (HET) spectrometer at the neutron spallation source ISIS with incoming energies of 20 and 60 meV, and energy resolutions of 0.6 and 1.8 meV in the 2.5 m detector banks. The low-angle banks cover $2\theta = 9° - 29°$ and the high-angle banks $130° - 140°$. All low- and high-angle detectors are grouped together, respectively, in order to gain statistics. We therefore refer to $S(2\theta,\omega)$ from now on. The corresponding averaged momentum transfers at elastic position for the low- and high-angle groupings are $\bar{Q} \approx 1.8$ Å^{-1} and ≈ 10.0 Å^{-1} for the 60 meV and $\bar{Q} \approx 1.0$ Å^{-1} and ≈ 5.5 Å^{-1} for the 20 meV data. Some data were taken at the cold time-of-flight spectrometer IN6 at ILL with an incoming energy of 3.1 meV and an energy resolution of 70 μeV at elastic position. All detectors from 10° to 115° have been grouped together. Because of the small incident energy the momentum transfer Q is ≤ 2 Å^{-1} in the energy window of interest. A flat sample geometry was used for all neutron experiments and—because of the enormous absorption of In, Rh, and Ir—well defined but thin samples were crucial in order to guarantee transmissions of at least 30%. This reduced the sample amount for the IN6 experiment to about 5 g. All data have been normalized to monitor count rate and vanadium and have been corrected for absorption and self-shielding. The description of the phonon correction has been moved to the appendix.

III. RESULTS

For Ce^{3+} in D_{4h} point symmetry the crystal-field Hamiltonian $H_{CF} = B_2^0 O_2^0 + B_4^0 O_4^0 + B_4^4 O_4^4$ describes the crystal-field potential when the three Stevens parameters B_2^0, B_4^0, and B_4^4 are determined. The B_k^m parameters are determined via the crystal-field transition energies within the Hund's rule ground state and the mixing parameter α. In Sec. III A the mixing parameter will be determined from the LD in the XAS data at low temperature, in Sec. III B the crystal-field energies are obtained from thermal neutron scattering data, and Sec. III C the order of crystal-field states will be confirmed from the temperature of the LD effect in the XAS spectra. In Sec. III D we finally present the quasielastic results from the cold neutron data in order to determine the hybridization temperatures T^*.

A. Low-temperature polarized soft XAS: the ground-state wave function

Figure 1 shows the low-temperature 20 K linear-polarized XAS data of $CeRhIn_5$, $CeIrIn_5$, and $CeCoIn_5$ at the Ce^{3+} $M_{4,5}$ edge full lines), i.e., at a temperature sufficiently low so that the ground state is populated. The latter has been verified with the knowledge of the crystal-field energies (see Table II). For $CeCoIn_5$ LD is smallest but has an opposite sign with respect to $CeIrIn_5$ and $CeRhIn_5$. $CeRhIn_5$ has the largest LD. Figure 1 shows further the simulations based on a full multiplet treatment as described in the experimental section (dotted lines). For $CeCoIn_5$ we find from our full multiplet calculation $\alpha = 0.36$. This value is just below the zero polarization for $\alpha = \sqrt{\frac{1}{6}} \approx 0.41$ where the LD vanishes when it changes sign. For $CeIrIn_5$ and $CeRhIn_5$ we obtain $\alpha = 0.50$ and $\alpha = 0.62$, respectively. The resulting ground-state wave functions, with an arbitrarily chosen phase, are

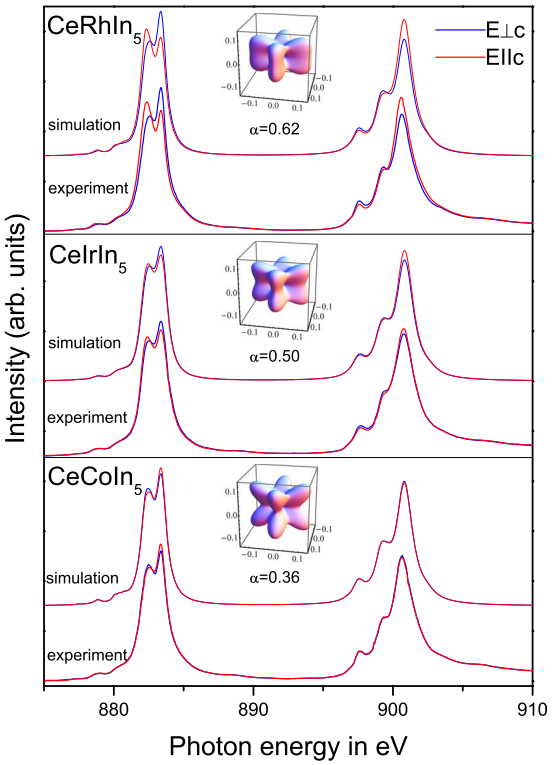

FIG. 1. (Color online) Low temperature ($T=20$ K) linear-polarized XAS spectra of $CeRhIn_5$, $CeIrIn_5$, and $CeCoIn_5$ at the Ce^{3+} $M_{4,5}$ edges. The solid lines are the measured data, the dotted ones the simulations as described in the text. The orbitals represent the spatial distribution of the $4f$ wave functions according to the respective ground-state admixtures, $\alpha|\pm 5/2\rangle + \beta|\mp 3/2\rangle$.

$$\text{CeRhIn}_5: \quad |0\rangle = \Gamma_7^2 = 0.62|\pm 5/2\rangle + 0.78|\mp 3/2\rangle,$$

$$\text{CeIrIn}_5: \quad |0\rangle = \Gamma_7^2 = 0.50|\pm 5/2\rangle + 0.87|\mp 3/2\rangle,$$

$$\text{CeCoIn}_5: \quad |0\rangle = \Gamma_7^2 = 0.36|\pm 5/2\rangle + 0.93|\mp 3/2\rangle.$$

The orbitals shown in Fig. 1 show the spatial distributions of the $4f$ electrons for the respective crystal-field ground states. The higher the $|5/2\rangle$ contribution to the ground state the flatter the $4f$ distribution, i.e., $CeRhIn_5$, which does not become superconducting at ambient pressure, has the flattest $4f$ orbital. The pure $|5/2\rangle$ orbital is donut and the pure $|3/2\rangle$ is yo-yo shaped (see e.g., Willers *et al.*[34]). The general trend of

TABLE II. Crystal-field energies $E_{1,2}$, widths (HWHM) $\Gamma/2$, and crystal-field parameters are given in meV. The fifth column gives instrument and incident energy E_{in} from which the parameters were determined. Values of $CeAu_2Si_2$ are shown for comparison. The crystal-field parameters from the full multiplet calculation are given in Stevens formalism.

(meV)	$CeRhIn_5$	$CeIrIn_5$	$CeCoIn_5$	Instrument (meV)	$CeAu_2Si_2$ (Refs. 15 and 36)
$\Gamma_{qu}/2$ @ 8 K	1.2 ± 0.2			IN6 3.1	0.13
$\Gamma_{qu}/2$ @ 75 K	1.7 ± 0.2	2.7 ± 0.5	3.9 ± 0.5	IN6 3.1	0.43
E_1	7.0 ± 0.5	5.2 ± 1.0	6.8 ± 1.0	HET 20	16.5
E_2	24.7 ± 1.0	29.4 ± 1.5	25.0 ± 1.5	HET 60	21.0
$\Gamma^1_{in}/2$ @ 5 K	1.6 ± 0.5	3.0 ± 0.5	4.8 ± 0.8	HET 20/60	
$\Gamma^2_{in}/2$ @ 5 K	1.8 ± 0.5	3.4 ± 0.8	4.7 ± 0.8	HET 60	
$\Gamma^1_{in}/2$ @ 75 K	2.5 ± 0.5	3.7 ± 0.5	4.4 ± 0.8	IN6 3.1	
B_{20}	−0.928	−1.197	−0.856		
B_{40}	0.052	0.069	0.063		
$\lvert B_{44}\rvert$	0.128	0.088	0.089		

a decreasing $|5/2\rangle$ contribution to the ground state from M =Rh and Ir to Co agrees with the INS findings by Refs. 31 and 32 but we observe smaller $|5/2\rangle$ contributions (note: $\sqrt{(1-\alpha^2)}=\beta$ as given by Christianson *et al.*). This is most likely due to systematic errors in the phonon correction of the INS neutron data (see appendix).

B. INS: crystal-field transition energies

Figure 2 shows the scattering function $S(2\theta,\omega)$ at T =5 K for small scattering angles $2\bar{\theta}=19°$ measured with two incident energies, E_{in}=20 meV (a)–(e) and 60 meV (f)–(h). The separation of magnetic and phonon correction has been performed as described in the appendix. E_{in}=20 meV: (a) and b) exhibit the scattering function $S(2\theta,\omega)$ of two nonmagnetic reference samples, and (c) and d) show $S(2\theta,\omega)$ of the three cerium compounds. The blue triangles are the total scattering. The data of the La samples show that there is only little phonon scattering for 20 meV incident energy. It has nevertheless been corrected for (method 2) in order to determine the magnetic scattering in the cerium data. The red

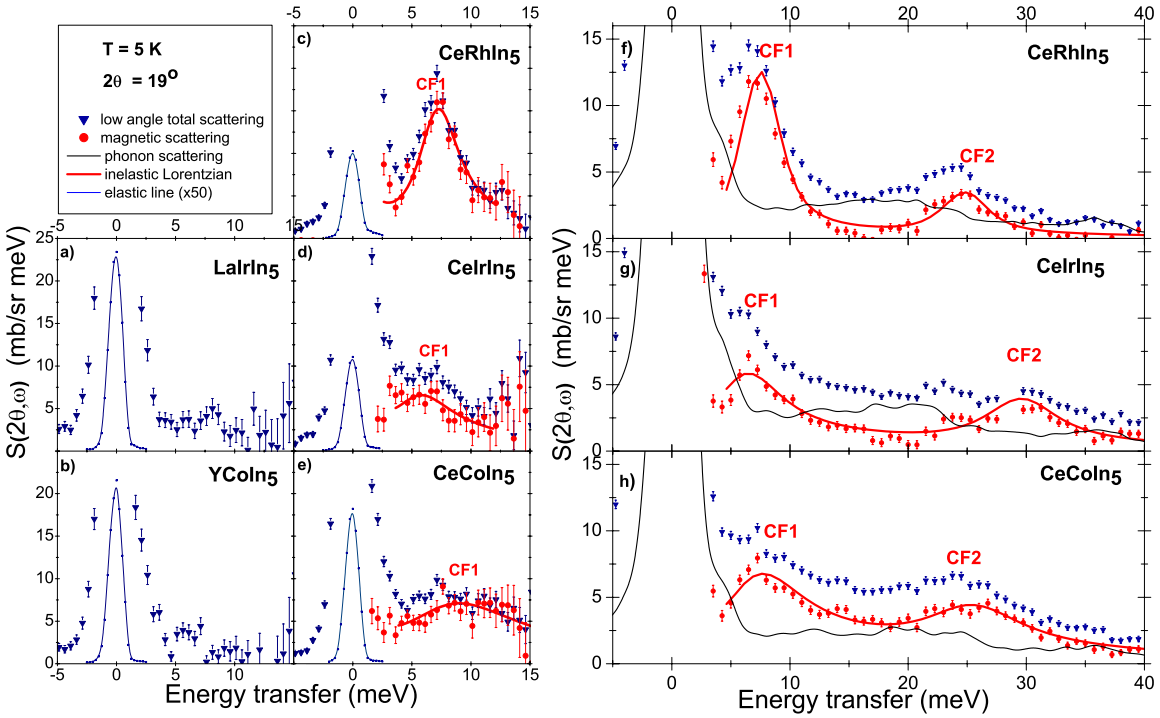

FIG. 2. (Color online) Inelastic neutron data at 5 K with 20 meV (a)–(e) and 60 meV (f)–(h) incident energy. The blue triangles represent the total scattering, the black lines the phonon intensities as obtained from a high to low angle scaling. The red circles show the magnetic scattering obtained after phonon correction (see appendix) and the red lines are Lorentzian fits.

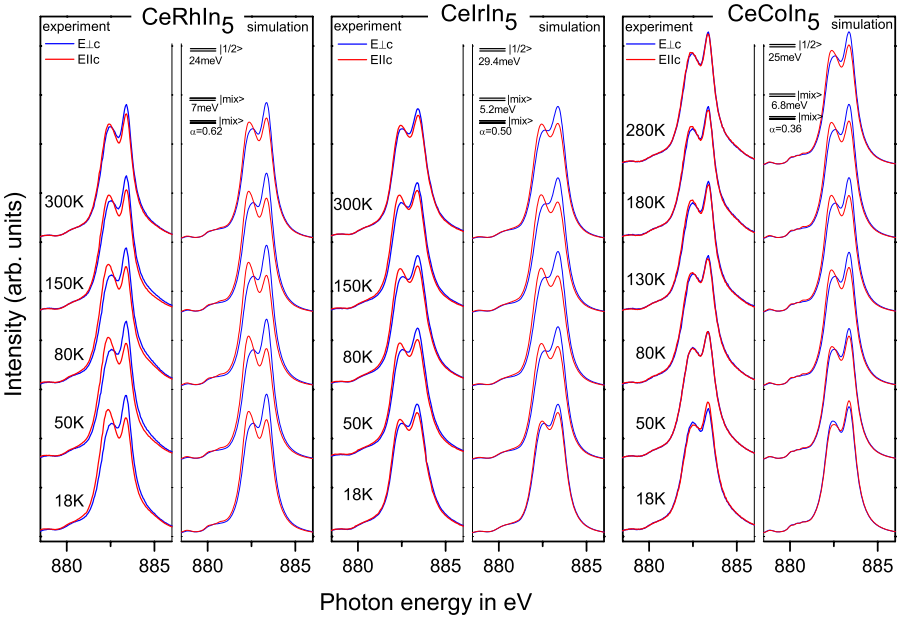

FIG. 3. (Color online) Left panel: temperature-dependent linear-polarized XAS spectra at the Ce^{3+} M_5 edge of $CeRhIn_5$, $CeIrIn_5$, and $CeCoIn_5$. The solid lines correspond to the measured data, the dotted lines to the simulation based on the crystal-field energies from the neutron data, and the ground-state wave functions from the low-temperature XAS data.

circles are the pure magnetic scattering after phonon correction. $E_{in}=60$ meV: the blue triangles in (f)–(h) are the total scattering for small scattering angles, i.e., for low Q and the black lines reflect the phonon scattering as obtained from the high to low-angle scaling method. The phonons scale with $R=1/8$ from $2\bar{\theta}=135°$ to $2\bar{\theta}=19°$ as empirically found from the nonmagnetic reference samples (see appendix). The red circles are the pure magnetic scattering in the low angle banks, resulting from subtracting the scaled phonon intensities (black lines) from the total scattering (blue triangles).

All three compounds exhibit two magnetic ground-state excitations at about 5–7 and 24–30 meV. The low-energy one (CF1) is best resolved in the 20 meV data while the 60 meV data show both excitations (CF1 and CF2). The quasielastic scattering cannot be resolved with these thermal measurements. The inelastic, magnetic excitations have been described with two inelastic Lorentzians. The crystal-field transitions are fairly sharp in $CeRhIn_5$ but much broader for $CeIrIn_5$ and $CeCoIn_5$, leading to considerable error bars in the line widths and position. The 60 meV data are described with two inelastic Lorentzians of same widths, but only the parameters of the higher energy excitations were freely varied, position and width of the low-energy excitations have been determined from the 20 meV data. We can state that the excitations broaden from $M=$Rh to Ir and Co. Table II gives the summary of all parameters.

In the $E_{in}=60$ meV data phonon and magnetic scattering are very much intermixed, the linewidths are broad and we know from the nonmagnetic reference samples that there is a substantial error in not taking out enough phonon scattering below 10 meV, i.e., in the range of the lower crystal-field excitation (this is explained in the appendix, see Fig. 6). We know further that the fine structure of the phonon scattering is not ideally represented by the Q scaled high-angle data (see appendix, right-hand panel of Fig. 6). Hence we do not attempt to determine magnetic intensities to obtain transition-matrix elements. The magnetic signal is nevertheless strong enough to determine the crystal-field energies fairly well, irrespective of the method of phonon correction as can be seen from the fact that we obtain similar line positions as Christianson *et al.* who applied some extra scaling factor for the phonon correction in addition to the one found from the La samples (compare appendix with Refs. 31 and 32). However, for $CeIrIn_5$ Christianson *et al.* can only state that the low-lying crystal-field state must be some where between 0 and 7 meV. Our neutron data show, due to the better flux and resolution, that the level is located between 5.2 ± 1 meV [see Fig. 2(e)]. This is supported by the fact that the polarization effect of the XAS data increases from 20 to 80 K (see Sec. III C, Fig. 3), i.e., when the thermal occupation of the first excited state takes place, before it decreases again due to the beginning population of the second excited state.

We find narrower linewidths and we find that the width of the spectra increases in the sequence $M=$Rh–Ir and becomes broadest for Co in contrast to Refs. 31 and 32. We believe that this is due to the better signal to noise ratio of the present data. While we do not consider the quality of the magnetic intensities to be sufficiently accurate to determine the wave functions properly from these data, we agree with Christianson *et al.*[31,32] that general intensity considerations based on the selection rule $\Delta J_z=\pm1$ lead to the conclusion that the $|5/2\rangle$ contribution to the ground state decreases from Rh to Ir and Co, that is in agreement with our low-temperature XAS data. We conclude further from the intensity ratios, as Chrstianson *et al.*,[31,32] that the second excited state is the pure $|1/2\rangle$ in all compounds.

The same set of data was taken at $T=120$ K (not shown here) where we would expect to see the transition from the first $|1\rangle$ to the second $|2\rangle$ excited state at E_2-E_1 but we do not resolve another peak. However, it should be noted that at 120 K the phonon correction is more important with respect to 5 K while the magnetic lines are broader. In addition, this third transition is weaker than the two ground-state excitations.

C. Temperature-dependent polarized soft XAS: sequence of crystal-field states

When analyzing the temperature dependence of the polarization-dependent XAS data we will only show the M_5 edge for clarity. Figure 3 shows the temperature dependence of the LD for all three cerium compounds. For each compound the measured data and corresponding simulations are shown. For $CeRhIn_5$ the LD in the experimental data increases slightly from 18 to 80 K indicating the population of the first excited crystal-field level and then decreases with further rising temperature due to population of the next state. When all states are equally populated the polarization should vanish entirely since an equal occupation resembles the fully degenerate Hund's rule ground state which has spherical symmetry. To the right of the measured data the simulated XAS spectra are shown. There, the crystal-field energies as determined in the neutron experiment and the mixing factor α as obtained from the low temperature XAS data are used as input parameters. The $|1/2\rangle$ has been assumed to be the highest-lying crystal-field level and only the population of states has been adapted to the corresponding temperature. The simulation reproduces well the trend of the temperature dependence of the LD, i.e., it increases at first and then decreases above 80 K with further rising temperature. The assumption of a different order of states would lead to a change of sign in the polarization for increasing T, which is in contradiction to the observation and can therefore be excluded. The other panels of Fig. 3 show the same set of spectra for $CeIrIn_5$ and $CeCoIn_5$. For $CeIrIn_5$ we observe very much the same effect as for $CeRhIn_5$ and we are able to simulate the general trend of the temperature dependence in the same manner. For $CeCoIn_5$ the temperature dependence seems different, but is based on the same effect, namely, occupation of the next higher states: the low-temperature polarization has a different sign with respect to M=Rh and Ir (see Sec. III A) so that here the occupation of the first excited state leads to a decrease in polarization with rising temperature and a change of sign between 50 and 80 K. Then the LD increases at first with further rising temperature and starts to decreases again above 180 K. Here too we are able to simulate this temperature trend under the assumption that the $|1/2\rangle$ is the highest-lying crystal-field state. For M=Co, the assumption of a different order of states would not give rise to a change of sign in the polarization as function of temperature. This analysis of the temperature dependence is analogous to our previous results on $CePt_3Si$.[34] Ground state, energy splittings, and order of states describe the crystal-field potential fully and the corresponding crystal-field parameters (in Stevens formalism) are listed in Table II.

While the temperature dependence of the LD is qualitatively reproduced with our simulations, there is also some quantitative deviation: at high temperatures the measured LD is always smaller than the simulated one. We exclude depolarization effects due to (a) surface degrading and/or (b) polycrystalline contributions. Possibility (a) can be excluded since we recleaved and repeated the measurements to assure reproducibility (see Table I) and we exclude (b) since it would require an unrealistic 35% of polycrystalline contribution in order to account for the mismatch in e.g., the Co data at 280 K. More physical and interesting is to consider Kondo interactions: they will have a depolarizing effect too. The hybridization of the $4f^1$ state with the surrounding conduction band has not been considered in the present analysis of the XAS data. Yet, the existence of the latter can be seen from the $4f^0$ initial state satellites at the high-energy tails of the $M_{4,5}$ edges. Figure 4 shows the isotropic spectra and the tails of the $M_{4,5}$ edges on a blown-up scale for the $CeMIn_5$ compounds and in comparison for $CeAu_2Si_2$. The arrows in Fig. 4 indicate the position of the f^0 spectral weight. $CeAu_2Si_2$ is an antiferromagnet with a small hybridization temperature (T^*=1.5 K) (Ref. 15) and with a good agreement of simulated and measured XAS data at all temperatures.[37] It is interesting to note that the $4f^0$ spectral weight is basically nonexistent in $CeAu_2Si_2$ but stronger in the $CeRhIn_5$ data and again more pronounced for $CeIrIn_5$ and $CeCoIn_5$. In the same sequence the inelastic line widths in the INS spectra and the deviation between simulated and measured spectra increase. We speculate that hybridization effects, which are not yet included in the calculation, may be responsible for these quantitative discrepancies. It is desirable that further theoretical work be carried out, using for instance the Anderson impurity model, to find out how much the CF wave functions are modified from our present estimates. We nevertheless expect that these modifications are very modest for the CeRhIn5 since the f^0 weight in the ground state is minimal. We may even speculate that the corrections are also small for the $CeCoIn_5$ and $CeIrIn_5$ in view of the special condition that the crystal-field ground-state wave function is very close to cubic, i.e., almost isotropic.

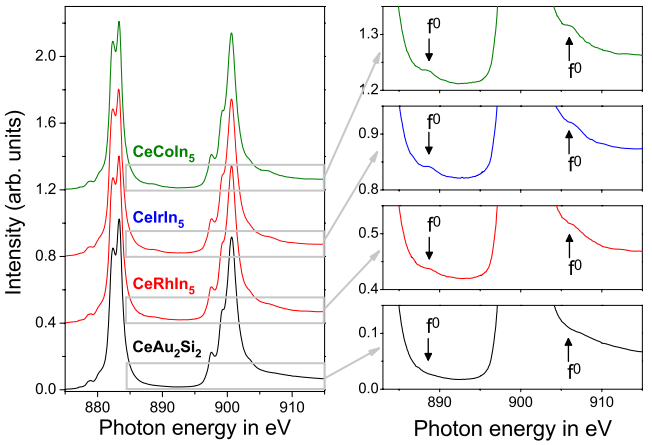

FIG. 4. (Color online) Isotropic spectra of $CeMIn_5$ with M=Rh, Ir, and Co, (at 20 K) and of $CeAu_2Si_2$ (at 40 K) for comparison. All spectra were recorded under the same beam line conditions at the NSRRC. In the right panel are blow-up graphs with arrows pointing out the $4f^0$ initial-state contributions.

D. INS: hybridization temperature T^*

Figure 5 shows high-resolution inelastic neutron scattering data of $CeMIn_5$ M=Rh, Ir, and Co, taken with IN6 at ILL

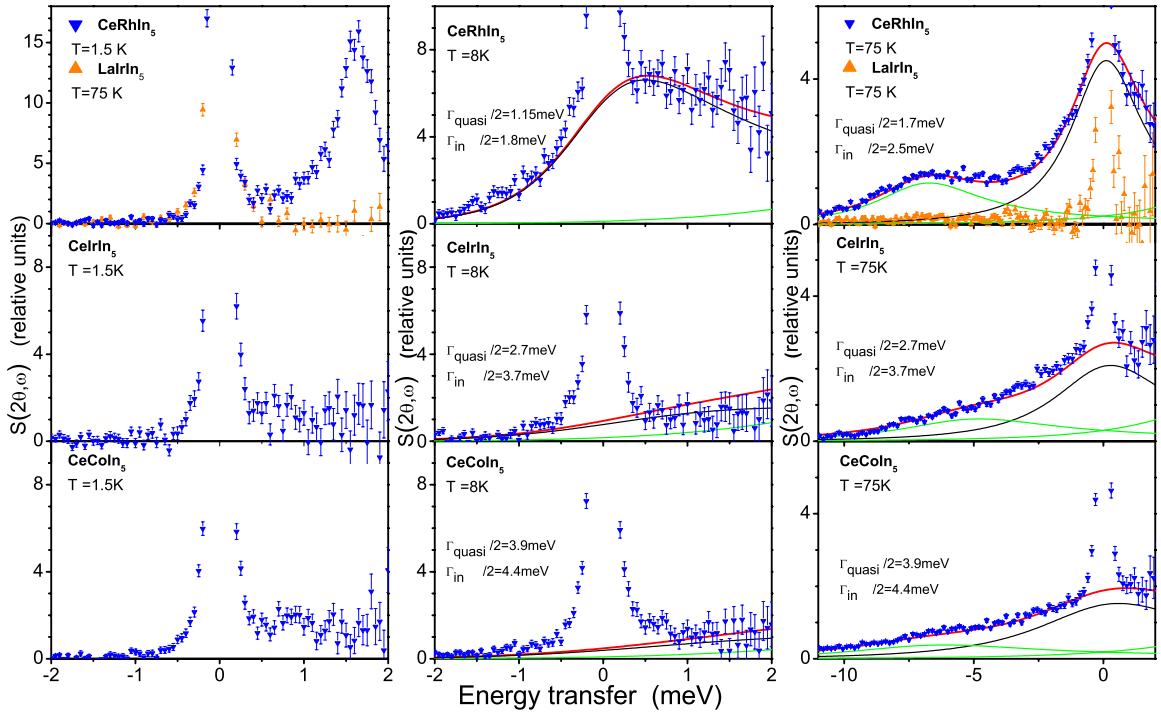

FIG. 5. (Color online) Neutron data with 3.1 meV incident energy. For $T=1.5$ and 8 K the neutron energy loss, for 75 K the neutron energy gain side is shown. The blue triangles (pointing down) are the total scattering of the cerium samples, the orange triangles (pointing up) are the La scattering. The 75 and 8 K data are described with one quasielastic (black) and one inelastic Lorentzian (green) with intensity ratios according to the crystal-field models (see Table II). The red lines reflect the total magnetic scattering.

with $E_{in}=3.1$ meV incident energy at 1.5, 8, and 75 K after background and absorption correction. The blue triangles (pointing down) are the total scattering from the cerium samples. We further show the scattering from $LaIrIn_5$ which was measured at 75 K. The La scattering, which is shown together with the 1.5 and 75 K $CeRhIn_5$ data, scatters around zero in the energy window up to 2 meV (see orange triangles in top left panel) and is negligible on the neutron energy gain side (see orange triangles in top right panel). We therefore neglect the phonon scattering.

At 1.5 K $CeRhIn_5$ is magnetically ordered ($T_N=3.8$ K) and the scattering function exhibits in addition to the elastic line (incoherent, elastic, nuclear scattering) some magnon density of states which peaks at about 1.7 meV. At 8 K the spectrum consists mainly of quasielastic scattering, which is well described with a quasielastic Lorentzian with half-width at half maximum (HWHM) $\Gamma/2=1.2(\pm 0.1)$ meV. Note, that for $\hbar\Gamma/2<k_BT$ a quasielastic Lorentzian appears highly asymmetric in energy.[38] The crystal-field excitation CF1 contributes only little in this energy window but has nevertheless been taken into account according to the crystal-field model (see green line). A quasielastic line width of $\Gamma/2=1.2(\pm 0.1)$ meV corresponds with $\hbar\omega=k_BT$ to $T^* \approx 14(\pm 1)$ K.

At 1.5 and 8 K the scattering intensity of $CeCoIn_5$ and $CeIrIn_5$ is considerably smaller with respect to $CeRhIn_5$, but it is not zero, as the comparison with the La data shows. It appears that there is some broad magnetic scattering in the data of either sample. Although $CeCoIn_5$ is in the superconducting phase at 1.5 K, we do not observe the spin resonance at 0.6 meV nor do we see the narrow 0.3 meV wide quasielastic line above the superconducting transition temperature, which were both seen in the single crystal data by Stock *et al.*[39] However, this is not a contradiction: as has been shown in detail by the authors of Ref. 39, the resonance at 1.3 K and its quasielastic precursor at 3 K are very local in reciprocal space. Both lines peak at (1/2; 1/2; 1/2). Our present data are not sensitive to such local scattering enhancement in reciprocal space although we cover this Q range $[(1/2;1/2;1/2)\equiv|Q|=1.048\ \text{Å}^{-1}]$ since our data are Q (powder) averaged and Q integrated ($0\ \text{Å}^{-1}\leq Q \leq 2\ \text{Å}^{-1}$). On the other hand, the broad magnetic, and apparent dispersionless signal which we observe in our Q averaged and integrated data will not have been observable in the single-crystal experiment where only one point in Q,ω space is probed at a time. The intensity would have appeared as some structure less background which is usually taken out in such experiments.[39] However, before attempting a more quantitative description of our 1.5 and/or 8 K data, the 75 K data shall be discussed.

At 75 K (see right column of Fig. 5) the energy window is larger due to population of states on the neutron energy gain side. Thanks to population and resolution the quasielastic scattering and the low-lying crystal-field excitation can be observed simultaneously in the same energy window. For $CeRhIn_5$ quasiscattering and inelastic scattering are well resolved while for $CeIrIn_5$ and $CeCoIn_5$ the spectra are substantially broader, which is in accordance with our observation at 1.5 and 8 K. We describe the data with the crystal-field model which we have obtained from the combined analysis of XAS and thermal neutron data, i.e., the intensity ratios of quasiline and inelastic line as well as the line posi-

tions are kept fixed (see parameters in Table II). Thus only the linewidths and an overall intensity parameter were varied. The latter is necessary although we attempted to scale to absolute intensities because the absorption corrections are so large. The data are well described with our crystal-field parameters, the resulting quasilinewidth and inelastic linewidth at 75 K are listed in Table II. Uncertainties come from the fact that in $CeIrIn_5$ and $CeCoIn_5$ quasiscattering and inelastic scattering are not well resolved due to the larger intrinsic linewidths.

We now return to the 8 K data of $CeIrIn_5$ and $CeCoIn_5$. If the broad magnetic scattering comes from the crystal-field ground state its intensity should differ from the Rh one according to the slightly different ground-state matrix elements in the Ir and Co sample. In order to find out whether the observed intensities in the 2 meV energy window correspond to scattering from the crystal-field ground state we now implement the description of the 75 K data to the 8 K data by only adjusting an over all scaling factor which we can pin to the $CeRhIn_5$ data at 8 K and by taking the respective matrix elements into account. Linewidths, positions were kept fixed to the values at 75 K and intensity ratios were given by the crystal-field model. The red lines in the 8 K spectra show the result of such an implementation. The red lines which correspond to scattering from the crystal-field ground state give a broad, nonzero contribution in the energy window up to 2 meV in agreement with our observation. The quantitative agreement (see red lines) is not perfect but satisfying. For $CeIrIn_5$ this attempt overestimates the scattering at 8 K, thus possibly referring to a slightly broader linewidths than deduced from 75 K. However, as mentioned above, this might be due to the fact that quasiscattering and inelastic scattering are not well resolved at 75 K, leading to considerable uncertainties in the linewidths. The $CeCoIn_5$ data are well described. This reasonable agreement verifies that the broad magnetic scattering is due to scattering from the crystal-field ground state and it gives us an estimate of the ground-state's width. We can conclude that the quasielastic linewidth at 8 K must be smaller than at 75 K but larger than 2.25 meV since at 8 K any narrower quasielastic line would peak within the present 2 meV energy window. 2.25 meV correspond to 26 K so that we summarize

$$CeRhIn_5: \quad T^* = 14 \pm 1 \ \text{K},$$

$$CeIrIn_5: \quad 26 \ \text{K} \leq T^* \leq 30 \pm 5 \ \text{K},$$

$$CeCoIn_5: \quad 26 \ \text{K} \leq T^* \leq 45 \pm 8 \ \text{K}.$$

IV. DISCUSSION

The hybridization temperatures T^* as determined from the present neutron-scattering experiments are smallest for $CeRhIn_5$ and largest for $CeCoIn_5$ in agreement with the increasing spectral weight of the f^0 contribution to the XAS spectra. The values we find from neutron scattering agree well with temperatures below which Fermi-liquid behavior sets in: the anomalous Hall effect below 20 K for $CeRhIn_5$, 31 K for $CeIrIn_5$, and 53 K for $CeCoIn_5$.[11] Knight-shift experiments give 10–12 K for $CeRhIn_5$, and for $CeCoIn_5$ 42 K for in plane, and 89–95 K for out of plane, i.e., a powder averaged value of about 58 K.[10] Thermal and transport measurements by Nakatsuji *et al.* give $T^* \approx 45$ K for $CeCoIn_5$ and the entropy of the specific heat of $CeRhIn_5$ reaches $1/2R \ln 2$ at about 10–12 K.[4] Our findings are further in agreement with the findings of the Fermi surfaces. While the general features of the Fermi surface of $CeRhIn_5$ are more like the Fermi surface of $LaRhIn_5$, which has no $4f$ electrons, the Fermi surfaces of $CeCoIn_5$ and $CeIrIn_5$ are well described with a more itinerant $4f$ band model.[30] A summary of values and references can be found in the supplementary information of Ref. 12.

$CeRhIn_5$ is the most localized member of this family. The hybridization temperature of $CeRhIn_5$ compares with those of other heavy-fermion materials like $CeCu_2Si_2$ ($T^* \approx 10$ K),[40] $CeRu_2Si_2$ ($T^* \approx 10$ K),[15] and with the ones of the antiferromagnetic compounds $CePd_2Si_2$ ($T^* = 10$ K, $T_N = 8$ K) (Ref. 15) and the cubic parent compound $CeIn_3$ ($T^* \approx 10$ K, $T_N = 10$ K).[5] With the exception of $CeRu_2Si_2$ all these compounds, exhibit superconductivity: $CeCu_2Si_2$ at ambient pressure depending on sample stoichiometry, or $CeRhIn_5$, $CePd_2Si_2$, and $CeIn_3$ with an applied pressure of 1.6 GPa and about 2.5 GPa for the latter two.[4,41,42] It is intriguing that for $CeAu_2Si_2$, which also orders antiferromagnetically at $T_N \approx 10$ K but has a much smaller hybridization temperature of $T^* = 1.5$ K,[15] no superconductivity has been reported up to 17 GPa.[43] Since pressure on the cerium ion increases delocalization, these findings underline the idea that sufficient Kondo screening favors superconductivity to the detriment of antiferromagnetic order.[6–8] For $CeIrIn_5$ and $CeCoIn_5$ where the hybridization temperatures are larger the Kondo screening seems to be sufficiently large so that superconductivity can develop at ambient pressure. Here the larger hybridization temperature of $CeCoIn_5$ ($T_c = 2.3$ K) with respect and $CeIrIn_5$ ($T_c = 0.4$ K) goes along with a higher superconducting transition temperature.

There is another aspect which makes $CeIrIn_5$ and $CeCoIn_5$ remarkable. They are rare examples for compounds where the hybridization temperature T^* is similar in magnitude to the size of the (low-lying) crystal-field splitting. One may speculate that this should have an effect on the degeneracies involved when describing ground-state properties.

Along with the increasing hybridization from $M = \text{Rh}$, via Ir to Co goes a decrease in the $|5/2\rangle$ contribution to the ground state. $CeRhIn_5$ which has the flattest $4f$ orbital (see orbitals in Fig. 2) does not become superconducting at ambient pressure and it does not appear in the T_c versus c/a scaling plot as suggested by Pagliuso[19] although its c/a ratio is in between the values of $CeIrIn_5$ and $CeCoIn_5$. The $CeIr_{1-x}Rh_xIn_5$ and $CeCo_{1-x}Rh_xIn_5$ systems, however, exhibit superconductivity and fit into this c/a scaling. It would be interesting to see where, in a similar scaling of T_c with the $4f$ wave functions, the $CeIr_{1-x}Rh_xIn_5$ and $CeCo_{1-x}Rh_xIn_5$ would fit. Since the crystal-field energies do not vary much from sample to sample it would be sufficient to determine the ground-state wave functions with linear-polarized XAS at low temperatures.

V. SUMMARY

We have determined the hybridization temperatures T^* and crystal-field schemes of CeMIn$_5$ M=Rh, Ir, and Co with inelastic neutron scattering and polarized soft x-ray absorption. The hybridization temperatures T^* as determined from the linewidths of the inelastic neutron data increase from M=Rh–Ir, and are largest for Co which supports the idea that increasing Kondo interaction favors superconductivity while preventing long-range magnetic order. The hybridization temperature of CeRhIn$_5$, the most localized member of the family, is comparable to the CeRu$_2$Si$_2$ and CeCu$_2$Si$_2$. For CeIrIn$_5$ and CeCoIn$_5$ the energy scale of the 4f conduction electron interaction is on the order of the energy of the low-lying crystal-field excitation, which may have an impact on the ground-state degeneracy and/or properties. Our finding of the crystal-field schemes is coherent with previous work by Christianson *et al.*[31,32] but we can give more precise values for the ground-state wave functions from our XAS data. We find that the $|5/2\rangle$ contribution to the ground state is largest (smallest) for CeRhIn$_5$ (CeCoIn$_5$) so that CeRhIn$_5$ has the flattest 4f orbital.

ACKNOWLEDGMENTS

The experiments at BESSY were supported by the BMBF under Project No. 05 ES3XBA/5. We thank L. Hamdan and the Cologne Mechanical Workshop for skillful technical support. The wave-function density plots and transition-matrix elements were calculated using the CrystalFieldTheory package for MATHEMATICA written by M. W. Haverkort.

APPENDIX

A single phonon-scattering process increases with momentum transfer Q as Q^2 and magnetic scattering decreases with the magnetic form factor of the magnetic ion. Phonon scattering follows Bose and the occupation of crystal-field states is according to Boltzmann statistics. We shall now discuss the two ways of separating magnetic and phonon scattering: (1) subtraction of the high-Q data from the low-Q data after scaling the high-Q data with a scaling factor R which has been determined with a nonmagnetic reference compound[14] and (2) subtraction of $S(Q,\omega)$ of a nonmagnetic reference which has been scaled by the average scattering cross section. Method (1): since we group angles and not momentum transfers Q we will determine the scaling factor for high to low scattering angles 2θ and not for Q. The left-hand panel of Fig. 6 shows $S(2\theta,\omega)$ of YCoIn$_5$ and LaIrIn$_5$ for 60 meV incident energy for large scattering angles 2θ=135° as black triangles (pointing up) and small scattering angles 2θ=19° as blue triangles (pointing down). All scattering of these nonmagnetic samples is of phonon origin so that a phonon scaling factor R from large to small scattering angles can be determined. Empirically we find for both nonmagnetic samples that the high-angle intensities scale to the low-angle ones with a factor of R=1/8. The quality of this scaling is shown in the right-hand panel of Fig. 6. The blue triangles (pointing down) are again the low-angle scattering, now shown on an expanded intensity scale

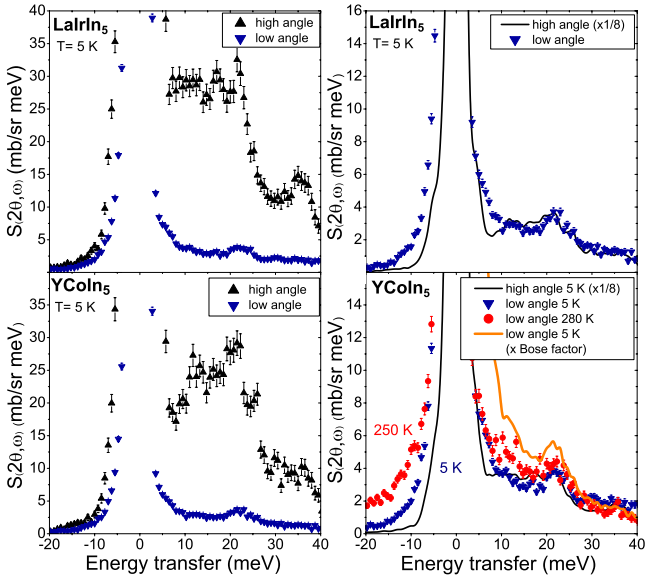

FIG. 6. (Color online) Inelastic neutron scattering data of the nonmagnetic reference compounds YCoIn$_5$ and LaIrIn$_5$. *Left*: high- and low-angle data at 5 K. *Right*: 5 K low-angle data shown on an expanded intensity scale and scaled (R=1/8) high-angle data. *Bottom right*: the red squares are the same low angle data taken at 280 K. The orange line represents the 5 K data scaled to 250 K with the Bose factor.

and the black line is the high-angle scattering scaled by R=1/8. While the overall intensity is well described, the low-angle phonon scattering below 10 meV is under estimated by such a scaling and the fine structure of the low-angle phonon scattering above 10 meV is not so well reproduced. Method (2): next we check method 2 by scaling the two nonmagnetic reference compounds to each other with the averaged nuclear cross section, again for grouped angles. The ratio of the averaged nuclear cross sections of YCoIn$_5$ and LaIrIn$_5$ is 1.37. For large scattering angles the 60 meV data seem to scale rather well with this value; we find a scaling factor of 1.3. However, for small scattering angles they do not. Here we find that the two nonmagnetic data sets scale best with a factor of 1.1. This deviation is probably due to multiple scattering which seems stronger in the forward detectors. This finding makes this type of scaling some what arbitrary for the magnetic samples unless a detailed phonon simulation and multiple scattering calculation is performed. Another obstacle of method 2 can be that often the nonmagnetic reference samples are only measured at base temperature and the higher temperatures are obtained from Bose scaling. The bottom-right panel of Fig. 6 shows that this can be traitorous: YCoIn$_5$ was measured at 5 (triangles) and 250 K (circles). Scaling the scattering function $S(2\theta,\omega,T)$ at 5 to 250 K with the Bose factor $[S(\theta,\omega,250\ \mathrm{K})=B(250\ \mathrm{K})/B(5)S(Q,\omega,5\ \mathrm{K})$ and $n(\omega,T)+1=B(T)=1/[1-exp(-h\omega/k_BT)]]$ gives the orange line which highly overestimates the actual scattering at 250 K. The Bose scaling does of course not take into account multiple phonon processes.

We therefore discard the direct subtraction method for the phonon correction of the 60 meV data and rather apply the

high to low Q or large to small scattering angle 2θ scaling. However, for the 20 meV data which exhibit very little phonon scattering in the forward detectors (see left column of Fig. 2) the cross-section scaling looks fine and we correct the 20 meV data by subtracting the data of the cross-section-scaled nonmagnetic reference samples since the high angle data of the 20 meV data contain still a non-negligible amount of magnetic scattering due to the smaller Q values.

*Present address: IFF, Research Centre Jülich, 52425 Jülich, Germany.

[1] C. Petrovic, P. G. Pagliuso, M. F. Hundley, R. Movshovich, J. L. Sarrao, J. D. Thompson, Z. Fisk, and P. Monthoux, J. Phys.: Condens. Matter **13**, L337 (2001).
[2] V. A. Sidorov, M. Nicklas, P. G. Pagliuso, J. L. Sarrao, Y. Bang, A. V. Balatsky, and J. D. Thompson, Phys. Rev. Lett. **89**, 157004 (2002).
[3] C. Petrovic, R. Movshovich, M. Jaime, P. Pagliuso, M. Hundley, J. Sarrao, Z. Fisk, and J. Thompson, Europhys. Lett. **53**, 354 (2001).
[4] H. Hegger, C. Petrovic, E. G. Moshopoulou, M. F. Hundley, J. L. Sarrao, Z. Fisk, and J. D. Thompson, Phys. Rev. Lett. **84**, 4986 (2000).
[5] W. Knafo, S. Raymond, B. Fak, G. Lapertot, P. Canfield, and J. Flouquet, J. Phys.: Condens. Matter **15**, 3741 (2003).
[6] P. Monthoux and G. G. Lonzarich, Phys. Rev. B **66**, 224504 (2002).
[7] P. Thalmeier and G. Zwicknagl, in *Handbook on the Physics and Chemistry of Rare Earths*, edited by K. A. Gschneider, Jr., J.-C. G. Bünzli, and V. K. Pecharsky, (Elsevier, North Holland, 2005), Vol. 34, and references therein.
[8] R. Flint and P. Coleman, arXiv:0912.2339 (unpublished).
[9] S. Nakatsuji, D. Pines, and Z. Fisk, Phys. Rev. Lett. **92**, 016401 (2004).
[10] N. J. Curro, B.-L. Young, J. Schmalian, and D. Pines, Phys. Rev. B **70**, 235117 (2004).
[11] Y. F. Yang and D. Pines, Phys. Rev. Lett. **100**, 096404 (2008).
[12] Y.-f. Yang, Z. Fisk, H.-O. Lee, J. D. Thompson, and D. Pines, Nature (London) **454**, 611 (2008).
[13] E. Holland-Moritz, D. Wohlleben, and M. Loewenhaupt, Phys. Rev. B **25**, 7482 (1982).
[14] A. P. Murani, J. Phys. C **16**, 6359 (1983).
[15] A. Severing, E. Holland-Moritz, and B. Frick, Phys. Rev. B **39**, 4164 (1989).
[16] J. M. Lawrence, P. S. Riseborough, C. H. Booth, J. L. Sarrao, J. D. Thompson, and R. Osborn, Phys. Rev. B **63**, 054427 (2001).
[17] A. P. Murani, A. Severing, and W. G. Marshall, Phys. Rev. B **53**, 2641 (1996).
[18] E. D. Bauer *et al.*, Phys. Rev. Lett. **93**, 147005 (2004).
[19] P. Pagliuso, N. Curro, N. Moreno, M. Hundley, J. Thompson, J. Sarrao, and Z. Fisk, Physica B **320**, 370 (2002).
[20] H. Weber and M. Vojta, Phys. Rev. B **77**, 125118 (2008).
[21] F. P. Mena, D. van der Marel, and J. L. Sarrao, Phys. Rev. B **72**, 045119 (2005).
[22] P. Ghaemi and T. Senthil, Phys. Rev. B **75**, 144412 (2007).
[23] K. S. Burch, S. V. Dordevic, F. P. Mena, A. B. Kuzmenko, D. van der Marel, J. L. Sarrao, J. R. Jeffries, E. D. Bauer, M. B. Maple, and D. N. Basov, Phys. Rev. B **75**, 054523 (2007).
[24] K. Kubo and T. Hotta, J. Phys. Soc. Jpn. **75**, 083702 (2006).
[25] J. Moreno and P. Coleman, Phys. Rev. Lett. **84**, 342 (2000).
[26] R. Flint, M. Dzero, and P. Coleman, Nat. Phys. **4**, 643 (2008).
[27] N. J. Curro, B. Simovic, P. C. Hammel, P. G. Pagliuso, J. L. Sarrao, J. D. Thompson, and G. B. Martins, Phys. Rev. B **64**, 180514(R) (2001).
[28] T. Takeuchi, T. Inoue, K. Sugiyama, D. Aoki, Y. Tokiwa, Y. Haga, K. Kindo, and Y. Ōnuki, J. Phys. Soc. Jpn. **70**, 877 (2001).
[29] S. Nakatsuji, S. Yeo, L. Balicas, Z. Fisk, P. Schlottmann, P. G. Pagliuso, N. O. Moreno, J. L. Sarrao, and J. D. Thompson, Phys. Rev. Lett. **89**, 106402 (2002).
[30] H. Shishido *et al.*, J. Phys. Soc. Jpn. **71**, 162 (2002).
[31] A. D. Christianson *et al.*, Phys. Rev. B **70**, 134505 (2004).
[32] A. D. Christianson, J. M. Lawrence, P. G. Pagliuso, N. O. Moreno, J. L. Sarrao, J. D. Thompson, P. S. Riseborough, S. Kern, E. A. Goremychkin, and A. H. Lacerda, Phys. Rev. B **66**, 193102 (2002).
[33] P. Hansmann *et al.*, Phys. Rev. Lett. **100**, 066405 (2008).
[34] T. Willers *et al.*, Phys. Rev. B **80**, 115106 (2009).
[35] A. Tanaka and T. Jo, J. Phys. Soc. Jpn. **63**, 2788 (1994).
[36] A. Severing, E. Holland-Moritz, B. D. Rainford, S. R. Culverhouse, and B. Frick, Phys. Rev. B **39**, 2557 (1989).
[37] T. Willers, Diploma thesis, University of Cologne, 2007.
[38] P. Fulde and M. Loewenhaupt, Adv. Phys. **34**, 589 (1985).
[39] C. Stock, C. Broholm, J. Hudis, H. J. Kang, and C. Petrovic, Phys. Rev. Lett. **100**, 087001 (2008).
[40] S. Horn, E. Holland-Moritz, M. Loewenhaupt, F. Steglich, H. Scheuer, A. Benoit, and J. Flouquet, Phys. Rev. B **23**, 3171 (1981).
[41] F. M. Grosche, S. R. Julian, N. D. Mathur, and G. G. Lonzarich, Physica B **223-224**, 50 (1996).
[42] N. D. Mathur, F. M. Grosche, S. R. Julian, I. R. Walker, D. M. Freye, R. K. W. Haselwimmer, and G. G. Lonzarich, Nature (London) **394**, 39 (1998).
[43] P. Link and D. Jaccard, Physica B **230-232**, 31 (1997).